

AppleVLM: End-to-end Autonomous Driving with Advanced Perception and Planning-Enhanced Vision-Language Models

Yuxuan Han¹, Kunyuan Wu¹, Qianyi Shao¹, Renxiang Xiao¹, Zilu Wang¹, Cansen Jiang³, Yi Xiao^{1*}, Liang Hu^{1,2*} and Yunjiang Lou¹

Abstract—End-to-end autonomous driving has emerged as a promising paradigm integrating perception, decision-making, and control within a unified learning framework. Recently, Vision-Language Models (VLMs) have gained significant attention for their potential to enhance the robustness and generalization of end-to-end driving models in diverse and unseen scenarios. However, existing VLM-based approaches still face challenges, including suboptimal lane perception, language understanding biases, and difficulties in handling corner cases. To address these issues, we propose AppleVLM, an advanced perception and planning-enhanced VLM model for robust end-to-end driving. AppleVLM introduces a novel vision encoder and a planning strategy encoder to improve perception and decision-making. Firstly, the vision encoder fuses spatial-temporal information from multi-view images across multiple timesteps using a deformable transformer mechanism, enhancing robustness to camera variations and facilitating scalable deployment across different vehicle platforms. Secondly, unlike traditional VLM-based approaches, AppleVLM introduces a dedicated planning modality that encodes explicit Bird’s-Eye-View spatial information, mitigating language biases in navigation instructions. Finally, a VLM decoder fine-tuned by a hierarchical Chain-of-Thought integrates vision, language, and planning features to output robust driving waypoints. We evaluate AppleVLM in closed-loop experiments on two CARLA benchmarks, achieving state-of-the-art driving performance. Furthermore, we deploy AppleVLM on an AGV platform and successfully showcase real-world end-to-end autonomous driving in complex outdoor environments.

Index Terms—End-to-End Autonomous Driving, Vision Language Model, Autonomous Vehicles, Imitation Learning

I. INTRODUCTION

Autonomous vehicles provide a promising solution to improve efficiency and mobility and thus play a vital role in modern intelligent transportation systems [1], [2]. Autonomous driving systems are typically classified into two paradigms: the end-to-end and the modular pipelines. The end-to-end paradigm takes environmental observation as input and directly outputs the control signals [3] or driving waypoints [4],

* Corresponding authors (Email: xiaoyi@hit.edu.cn; l.hu@hit.edu.cn).

¹ Y. Han, K. Wu, Q. Shao, R. Xiao, Z. Wang, Y. Xiao, L. Hu and Y. Lou are with Shenzhen Key Lab for Advanced Motion Control and Modern Automation Equipments, Guangdong Provincial Key Laboratory of Intelligent Morphing Mechanisms and Adaptive Robotics, School of Intelligence Science and Engineering, Harbin Institute of Technology, Shenzhen, China.

² L. Hu is also with National Key Laboratory of Smart Farm Technologies and Systems, China.

³ C. Jiang is with Autonomous Driving Center, Shanghai Utopilot Technology Co.Ltd., China.

streamlining the training process and reducing data labeling costs. As a result, this paradigm has witnessed a rapid advancement in recent years [5].

Early end-to-end approaches were vision-based, aiming to learn driving behaviors directly from raw visual observation. Two widely used learning methods in this paradigm are: *Reinforcement Learning (RL)* [6] and *Imitation Learning (IL)* [7]. RL-based approaches learn driving policies through trial and error using handcrafted reward functions, whereas IL leverages expert demonstrations to map observations to driving actions without explicitly defining a reward function. IL does not face the issues of sparse rewards and does not require manually defining an explicit reward function (which can be extremely complicated in certain scenarios), and hence has shown promising performance in autonomous driving [8].

However, relying solely on visual input is insufficient for real-world driving. For instance, when approaching an intersection, navigation instruction is essential to indicate the correct direction; similarly, in emergency scenarios such as pedestrians crossing, contextual warnings can improve safety [9]. To address such limitations, Vision Language Models (VLMs) have been introduced in autonomous driving models [10], integrating the inputs of both vision and language modalities. By leveraging the power of foundation models such as CLIP [11] and Large Language Models (LLMs) [12], the VLMs enhance understanding and reasoning in complex driving scenarios [13]. Typically, a VLM-based driving framework consists of three modules: 1) an input encoder that tokenizes the vision and natural language inputs as a sequence of multi-modal representation; 2) a language model that processes these tokens to generate driving decisions in text form; 3) an information decoder that converts these decisions into driving waypoints and control signals for driving [14]. In contrast to Vision-Language-Action (VLA) models [15], [16] that directly regress actions (e.g., control signals) from inputs, we adopt VLMs along with an extra controller to provide explicit reasoning and improve interpretability [17].

LMDrive [18] pioneered the use of LLMs for closed-loop autonomous driving. Though the existing end-to-end autonomous driving models show strong capabilities to handle complex instructions and challenging driving scenarios in the CARLA simulator, they still struggle in real-world applications [19], [20]. Specifically, end-to-end autonomous driving models are sensitive to sensor configuration such that even minor variations in sensor placements and resolutions

can significantly impact perception, limiting the scalability across different vehicles. Furthermore, the natural language, as an abstract expression, lacks spatial precision and might cause understanding ambiguity. For instance, an instruction like “Go straight at the intersection” may not specify which lane to take when merging onto a multi-lane road, causing unintended lane oscillations. Moreover, current VLM-based driving models are pre-trained on standard driving datasets, making them ineffective in handling rare yet critical cases such as a sudden pedestrian crossing.

To overcome these challenges, we propose a novel model called AppleVLM, short for Advanced Perception and PLanning-Enhanced Vision-Language Models for end-to-end autonomous driving. AppleVLM follows the IL method, trained from a set of expert driving data for closed-loop driving. Our contributions can be summarized as follows:

- 1) We introduce a novel end-to-end driving framework that is more robust to sensor configurations and resolutions, highlighting its potential as a scalable solution for real-world deployment across diverse vehicle platforms;
- 2) The proposed vision encoder employs a deformable attention mechanism to fuse RGB images and point-cloud data across both spatial (multi-view) and temporal (multi-timestep) dimensions, which significantly improves lane perception accuracy and enhances robust waypoint prediction;
- 3) We propose a planning strategy encoder to explicitly represent driving scenarios. With the planning features, the model can significantly mitigate language-induced perception biases and improve interpretability;
- 4) The real-world corner-case datasets are used to fine-tune the VLM backbone with Chain-of-Thought (CoT). It enables our model to involve more out-of-distribution data, thus achieving better generalization performance in both simulation and the real world.

II. RELATED WORK

A. End-to-End Imitation Learning

End-to-end autonomous driving has gained significant attention due to its simplicity in training and the benefit of not requiring manual data labeling [7], [21]. Current end-to-end driving models apply either RL or IL methods [22]–[24]. Designing effective reward functions to address diverse scenarios in open-world settings remains a challenge in RL, and its initial training and testing are quite dangerous. In comparison, IL has been more widely studied as an alternative.

Existing end-to-end IL models in autonomous driving have two types of output: action and waypoint. The action-based end-to-end driving models [3], [25], [26] directly map observation to vehicle control action, offering a straightforward solution without requiring controller design. On the other hand, the waypoint-based end-to-end driving models [4], [21], [27], [28] output waypoints from observation, and then a controller is designed and tuned to transform trajectory waypoints to vehicle control, which provides a clearer understanding of decision-making and better diagnostics. To take both advantages, TCP [29] integrates trajectory planning and direct control by two

branches, with one predicting future waypoints while the other one reasoning multi-step actions. Recently proposed Transfuser++ [21] discusses these two types of end-to-end models and achieves more robust results in the waypoint-based ones. Therefore, in this work, we focus on the waypoint-based end-to-end models.

Early end-to-end driving models rely on uni-modal vision input. Transfuser [27] pioneers the deep fusion of image and point-cloud features using hybrid transformer-CNN architectures, achieving remarkable waypoints prediction results on the Longest6 [30] benchmark. InterFuser [28] further improves accuracy by using a single transformer for vision encoding and waypoint decoding. UniAD [4] is the first work of full-stack driving architecture that generates waypoints for vehicle navigation in the real world. These vision-based uni-modal models demonstrate the feasibility of end-to-end driving, however, they only focus on feature extraction in images but lack the direct understanding of semantic information, which makes it difficult to understand abstract concepts in complex scenes. To bridge this gap, multi-modal vision-language models have emerged as promising paradigms, including VLA and VLM [17]. VLA models [15], [16] that directly map vision-language inputs to actions have gained traction for their training simplicity. In contrast, the VLM-based approaches provide explainable decision-making through natural language and planning strategy, as summarized in [17].

B. VLMs in Driving

In recent years, VLMs have attracted widespread attention due to their ability to integrate multi-modal information (*i.e.* vision and language) for better understanding and reasoning in autonomous driving [31]–[33]. DriveGPT-4 [34] introduces a multi-modal VLM that takes a sequence of image frames and human questions as input, and outputs control signals and answers. However, it lacks the input of navigation instructions, thus cannot drive following planned routes. Moreover, it was evaluated on open-loop datasets, which might cause the covariate shift problem that occurs gradually over time or during real-world deployment. DriveLM [35] builds upon nuScenes and CARLA, and proposes a VLM-based approach for jointly performing graph visual question-and-answer and end-to-end driving. DriveVLM [36] takes images as input and outputs scene description, scene analysis, and hierarchical planning results through a CoT mechanism, achieving enhanced scenario understanding. LMDrive [18] is the very first work to leverage LLMs and shows promising performance in closed-loop end-to-end driving.

These works have demonstrated the promising potential of VLMs in end-to-end driving, however, several limitations remain to be addressed for performance improvement. Firstly, existing VLMs for autonomous driving exhibit high sensitivity to sensor configurations during training and testing. In other words, even minor variations in sensor positioning and orientation can significantly impact driving performance. Secondly, VLMs exhibit inherent language biases, where ambiguous or imprecise language expressions may lead to misinterpretations of driving scenarios. Incorporating more explicit feature rep-

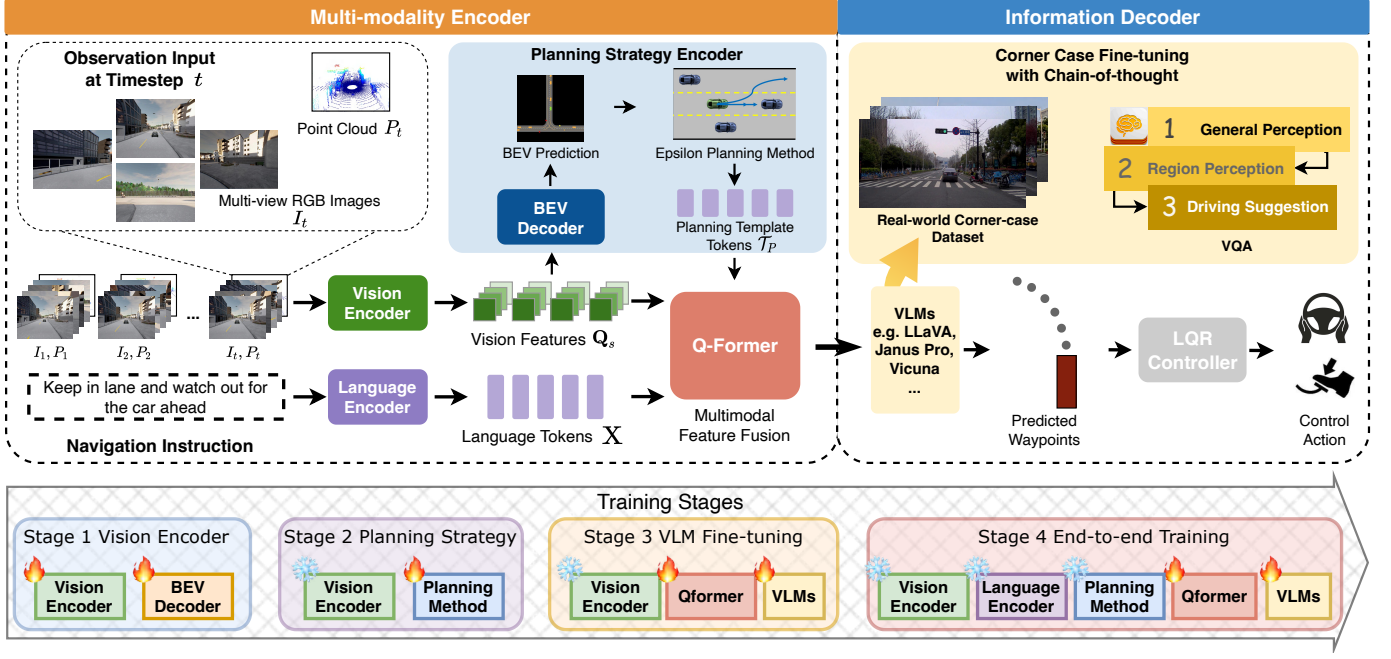


Fig. 1: The proposed AppleVLM follows an encoder-decoder architecture: The **Multi-modality Encoder** includes three types of encoders: 1) a vision encoder processes a time sequence of multi-view sensor data (RGB images and point-cloud) and generates vision features; 2) a language encoder encodes the navigation instructions to language tokens; 3) a planning strategy encoder takes vision features as input and outputs the planning template tokens. These features from three modalities are fused by a module based on the Q-Former architecture. The **Information Decoder** adopts a VLM backbone (such as LLaVA or Janus Pro) to process the multi-modal features. This VLM is pre-trained with corner-case data following a CoT mechanism with three tasks: general perception, region perception, and driving suggestion to predict a sequence of driving waypoints. During the training process of end-to-end driving, the fine-tuned VLM is frozen, and an LQR controller is adopted to transform waypoints to control actions for actual driving, *i.e.* steering angle, throttle and brake. The training process consists of four stages: **stage 1** is pre-training the vision encoder for BEV prediction; **stage 2** is learning the planning strategy with features from the frozen vision encoder; **stage 3** is fine-tuning the VLM with Q-Former on corner-case data with CoT mechanism; and in **stage 4**, the end-to-end training leveraging features from all frozen encoders, and the trainable Q-Former and VLM.

resentations may mitigate the issue. Moreover, current closed-loop VLMs do not cover corner-case driving scenarios in model training, which is more likely to lead to covariate drift in real-world driving.

III. METHODOLOGY

A. Problem Setting

To train the AppleVLM, we follow the IL method, where the idea is to train an agent that drives with a policy π that imitates the policy of an expert driver π^* . The policy π is trained in a supervised manner following the behavior cloning [1] approach of IL. In this work, as we focus on waypoint-based end-to-end driving, the policy is a mapping from observation to waypoints, which are then fed to a separate controller and output driving control actions.

Before training an agent, we allocate an expert driver in the environment to generate a dataset $\mathcal{D} = \{(\mathbf{O}_l, \mathbf{W}_l)\}_{l=1}^L$ of size L , which consists of high-dimensional observation of the environment \mathbf{O} , and the corresponding expert driving trajectories represented by a set of 2D waypoints in Bird's-Eye-View (BEV) space $\mathbf{W} = \{(x_t, y_t)\}_{t=1}^T$ where T is the number of predicted waypoints at each time step. This dataset

is then used to train a parameterized policy $\pi_\theta(\cdot)$, which approximates the expert policy. The training objective is:

$$\arg \min_{\theta} \mathbb{E}_{(\mathbf{O}_l, \mathbf{W}_l) \sim \mathcal{D}} [\mathcal{L}(\pi_\theta(\mathbf{O}_l), \mathbf{W}_l)]. \quad (1)$$

Overall, the training process of AppleVLM consists of four stages: 1) *Vision Encoder Pre-training with BEVs*: we use BEV prediction as a pre-training task for the vision encoder, aiming to encode spatial information for better vision feature extraction; 2) *Planning Strategy Encoder Training*: the output features of the vision encoder is used as input to train the planning strategy encoder, where a set of spatial-temporal corridors are generated; 3) *VLM Fine-tuning with Corner Cases*: we use a real-world corner-case dataset to fine-tune the VLM baseline to alleviate the long-tail problem of training data; 4) *End-to-end Training of AppleVLM*: the pre-trained vision encoder and planning strategy encoder are frozen, while the rest part of the model is end-to-end trained for the driving task. The corresponding losses are described in III-C.

B. Architecture

As shown in Fig. 1, the proposed AppleVLM comprises a *Multi-modality Encoder* and an *Information Decoder*. We will

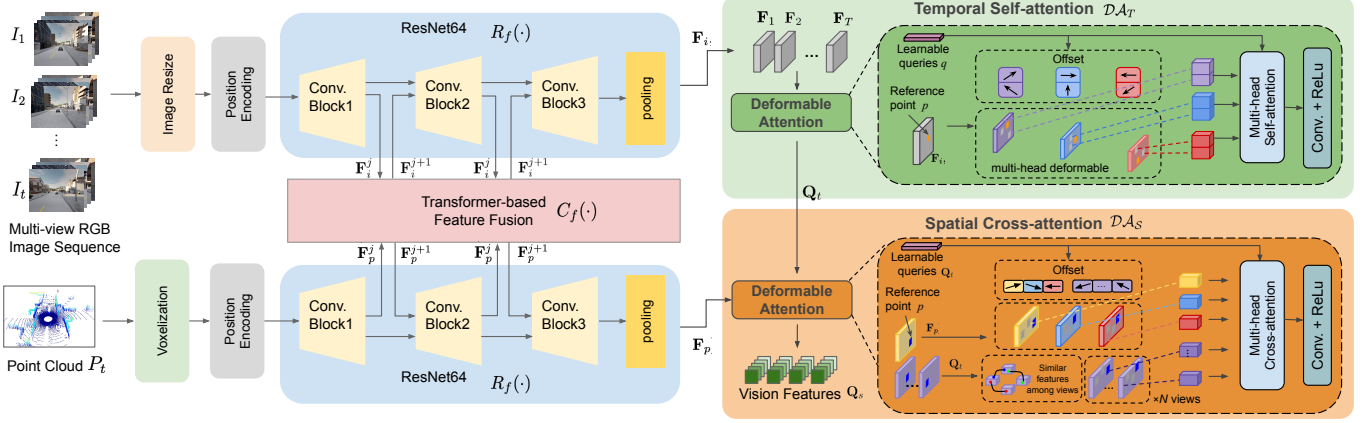


Fig. 2: Details of the vision encoder. The features of images and the point cloud are fused by the self-attention mechanism at several convolution blocks in the ResNet64 backbone. Furthermore, a deformable self-attention mechanism is applied to the image feature sequence over T frames, and a deformable cross-attention mechanism is adopted to associate features from the modalities of images and the point cloud.

introduce these two modules in III-B1 and III-B2, respectively, and finally describe the training details in III-C.

1) *Multi-modality Encoder*: AppleVLM consists of encoders that incorporate features from three modalities: vision, language, and planning strategy.

Vision Encoder: Fig. 2 shows the details of the vision encoder. The perception input \mathbf{O} consists of a sequence of multi-view RGB images $\mathbf{I} = \{I_{t,1}, I_{t,2}, \dots, I_{t,N}\}_{t=1}^T$ (T and N are numbers of time-step and view), and the point cloud data $\mathbf{P} = \{P_1, P_2, \dots, P_t\}_{t=1}^T$. To align the dimension of perception input data, we apply bilinear interpolation on \mathbf{I} to normalize the image size, and voxelization on \mathbf{P} , which is further processed to pseudo image $\mathbf{I}_p = \phi(\mathbf{P})$. We use two ResNet64 backbones $R_f(\cdot)$ to extract features \mathbf{F}_i and \mathbf{F}_p from \mathbf{I} and \mathbf{I}_p respectively, described as below:

$$\begin{aligned} \mathbf{F}_i &= R_f(\mathbf{I}), \quad \mathbf{F}_p = R_f(\phi(\mathbf{P})), \\ \mathbf{F}_i^{j+1} &= [\mathbf{F}_i^j, \mathbf{F}_p^j] = C_f(\mathbf{F}_i^j, \mathbf{F}_p^j). \end{aligned} \quad (2)$$

For each convolutional block in $R_f(\cdot)$, we take the feature output at current block j , \mathbf{F}_i^j and \mathbf{F}_p^j , and consecutively obtain \mathbf{F}_i^{j+1} and \mathbf{F}_p^{j+1} by the feature fusion function $C_f(\cdot)$ in the Transformer with shared weights. Through the cross-attention mechanism, we fuse the features from different modalities of vision input.

Once the fused feature $\mathbf{F} = [\mathbf{F}_i, \mathbf{F}_p]$ is obtained via (2), we further process it through a temporal self-attention block and a spatial cross-attention block built upon the Deformable Attention (\mathcal{DA}) [37], which is formally described as below:

$$\mathbf{Q} = \mathcal{DA}(q, p, \mathbf{F}) = \sum_{m=1}^M \sum_{k=1}^K \mathcal{A}_{mk} \cdot \mathcal{W}_m(q) \cdot \mathbf{F}(p + \Delta p_{w,h})$$

where q is the query, p is the reference point, and $\Delta p_{w,h}$ represents the predicted offsets regarding to p , M and K indicate the numbers of the attention heads and the sampled keys in each head, respectively. \mathcal{W}_m represents the learnable weights in head m , and \mathcal{A}_{mk} is the predicted attention weight. This enhanced attention mechanism dynamically adjusts the

region of interest by introducing deformable offsets and thus can flexibly capture important features across multiple heads.

Based on the idea of \mathcal{DA} , for \mathbf{F}_i that contains features of the T timesteps, we apply a temporal self-attention block \mathcal{DA}_T to associate features among the sequence and obtain \mathbf{Q}_t as below:

$$\mathbf{Q}_t = \mathcal{DA}_T(q, p_f, [\mathbf{F}_i^1, \dots, \mathbf{F}_i^T]) = \sum_{t=1}^T \mathcal{DA}(q, p_f, [\mathbf{F}_i^t]),$$

then the temporal fused feature of all views \mathbf{Q}_t , along with the feature output of the point cloud branch \mathbf{F}_p are fed into a spatial cross-attention block \mathcal{DA}_S :

$$\begin{aligned} \mathbf{Q}_s &= \mathcal{DA}_S(\mathbf{Q}_t, p_f, (\mathbf{Q}_t, \mathbf{F}_p)) \\ &= \left(\frac{1}{|\mathcal{V}_{\text{hit}}|} \sum_{m \in \mathcal{V}_{\text{hit}}} \mathcal{DA}(\mathbf{Q}_t, p_f, \mathbf{Q}_t \in m) \right) + \mathcal{DA}(\mathbf{Q}_t, p_f, \mathbf{F}_p) \end{aligned}$$

In this block, we take the \mathbf{Q}_t as the query, and m views with similar features in \mathbf{Q}_t , *i.e.* \mathcal{V}_{hit} , as the key, to apply the cross-attention feature fusion. Next, the same \mathcal{DA} is applied while using the point cloud feature output \mathbf{F}_p as the key. Finally, these features are concatenated as the final feature output of the vision encoder, \mathbf{Q}_s .

Notably, our proposed vision encoder can adapt variations in sensor configurations (*i.e.* position, orientation) due to the deformable attention mechanism, which adaptively adjusts the sampling position to capture changes in the scene. This bypasses cumbersome camera calibration and increases model generalization during real-world deployment.

Language Encoder: The navigation instruction is built upon the LMDrive, which consists of three specific scenarios (*e.g.* follow, turn, and others) [18]. To process the input data of the language encoder, we follow the conventional natural language processing procedure, splitting the navigation instruction into tokens, such as words and sub-words, and removing the punctuation. Then, these tokens are mapped to a vector of input sequence $\mathbf{X} = (x_1, x_2, \dots, x_n)$ by Word2Vec [38]

Finally, special tokens (e.g. [CLS], [Distance]) are added to the sequence \mathbf{X} as specific features for autonomous driving.

Planning Strategy Encoder: Different from most existing VLM-based autonomous driving models, AppleVLM incorporates a novel planning strategy encoder that leverages the explicit representation of the environmental information, *i.e.*, lane perception and the states of surrounding objects, to reduce the bias caused by the implicit representation of navigation instructions in natural languages. Specifically, we decode the output feature of the vision encoder \mathbf{Q}_s with a BEV decoder consisting of several convolutional layers and multi-layer perceptron (MLP) to output BEV semantic segmentation images $\mathbf{B} \in [0, 1]^{H_g \times W_g \times C_g}$, consisting of C_g grayscale images of size $H_g \times W_g$. In our case, we consider $C_g = 3$, including semantic grayscale images of the drivable area \mathcal{X} , the lane boundary \mathcal{E} , and the state of the surrounding objects \mathcal{S} .

Based on this environmental information, we adopt the Epsilon [39] planning method $\mathcal{P}_e(\cdot)$ to generate driving trajectories and candidate driving corridors with high scores of success and safety in the scene, as depicted in Fig. 3. Specifically, the top N policies \mathbb{T}^p generated by $\mathcal{P}_e(\cdot)$ are selected, that is

$$\mathbb{T}^p = \arg \max_{x_{t_H}^1, x_{t_H}^2, \dots, x_{t_H}^i} (\mathcal{P}_e(\mathcal{X}, \mathcal{E}, \mathcal{S}))$$

This representation explicitly offers temporal and spatial geometry information of the driving scene, thereby mitigating language biases induced by abstract navigation instruction.

With \mathbb{T}^p , we transform them into a three-dimensional tensor $\mathbb{P}^p = [T, X, Y]$, where the temporal dimension T and the spatial occupancy grid $[X, Y]$ of corridors at time T are encapsulated. We concatenate different policies tensor as a whole in $[\mathbb{P}^p]$. Then, we apply a Spatial-Temporal Transformer Tokenizer [40] **Token**(\cdot) to encode $[\mathbb{P}^p]$ to planning template tokens \mathcal{T}_P , that is $\mathcal{T}_P = \text{Token}([\mathbb{P}^p])$ where $p \in N$.

Multi-modality Feature Fusion: As illustrated in Fig. 4, we integrate vision features, language tokens, and planning template tokens by a Querying Transformer (Q-Former) [41] architecture. We first apply cross-attention $\mathcal{A}_{cross}(\cdot)$ to obtain two fused features: *perception* feature $\mathbf{F}_{perception}$ that are fused by vision features and planning template tokens, and *command* feature $\mathbf{F}_{command}$ that are fused by language and planning template tokens as below:

$$\begin{aligned} \mathbf{F}_{perception} &= \mathcal{A}_{cross}(\mathbf{Q}_s, \mathcal{T}_P) \\ \mathbf{F}_{command} &= \mathcal{A}_{cross}(\mathbf{X}, \mathcal{T}_P) \end{aligned}$$

Then $\mathbf{F}_{perception}$ and $\mathbf{F}_{command}$ are fed into the Q-Former with the learnable queries. The idea is to extract meaningful and most relevant features from $\mathbf{F}_{perception}$ and convert them into a format that can be effectively fused with $\mathbf{F}_{command}$, achieving the alignment of the features from different modalities. Finally, the outputs of the Q-former are concatenated and passed to an MLP module to obtain encoded feature \mathbf{F}_m .

2) *Information Decoder:* Before the end-to-end training of AppleVLM, the VLM backbone is pre-trained through a CoT mechanism with three tasks: general perception, region perception, and driving suggestion. When training the end-to-end AppleVLM, the fine-tuned VLM is frozen, and the

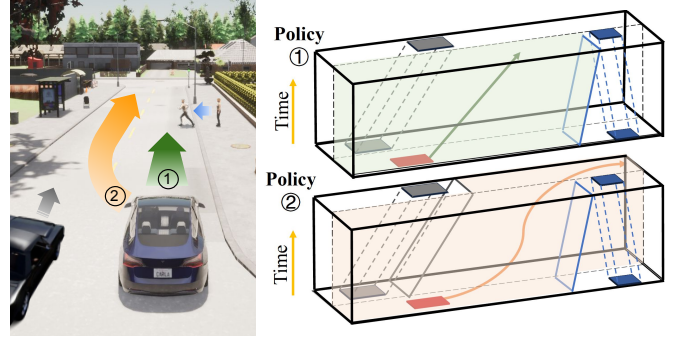


Fig. 3: An example of a driving scenario is shown on the left. By applying the Epsilon [39] planning method, the corridors that represent the possible driving space along time are generated on the right. Corridors of the other vehicle and pedestrian are illustrated in gray and blue respectively. The red rectangle indicates the initial location of the ego vehicle. By integrating the top N policies (the orange and green lines), we conduct a constraint corridor for the ego vehicle.

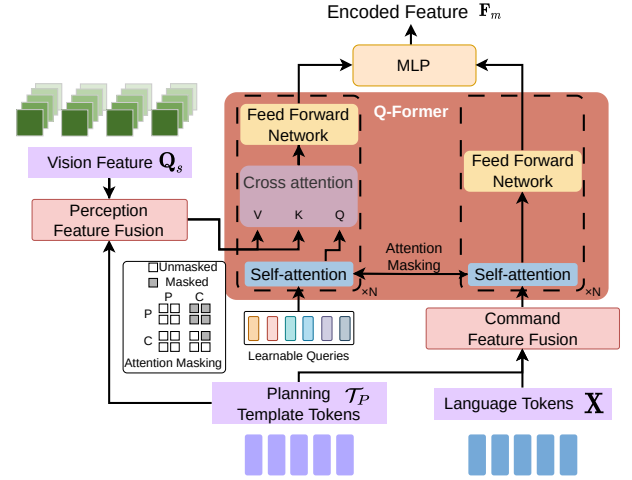


Fig. 4: The planning template tokens \mathcal{T}_P encoded from explicit representation (*i.e.* the spatial-temporal corridor) of the driving scene are fused into the vision and language features by a Q-former-based architecture.

encoded feature \mathbf{F}_m is fed into the VLM. Then, the VLM outputs a set of driving waypoints, which are further processed by a control model to produce vehicle control actions: steering angle, throttle, and brake.

VLM pre-trained with CoT: We choose the latest proposed model, Janus Pro [42], as the VLM backbone. Considering that autonomous driving models need to be rolled out in a wide range of driving scenarios, including rare or unexpected situations, we fine-tune the VLM with driving-specific corner-case data [43] that is not well-represented in standard training datasets. Inspired by [43] and [35], the fine-tuning contains a CoT process with three tasks: 1) *General Perception*, where the task is to understand which kinds of critical entities are on the road, and the reasons why they influence the driving behaviors of the ego vehicle; 2) *Region Perception*, where the task is to describe objects within the given bounding boxes and explain why they would influence the ego vehicle's behavior;

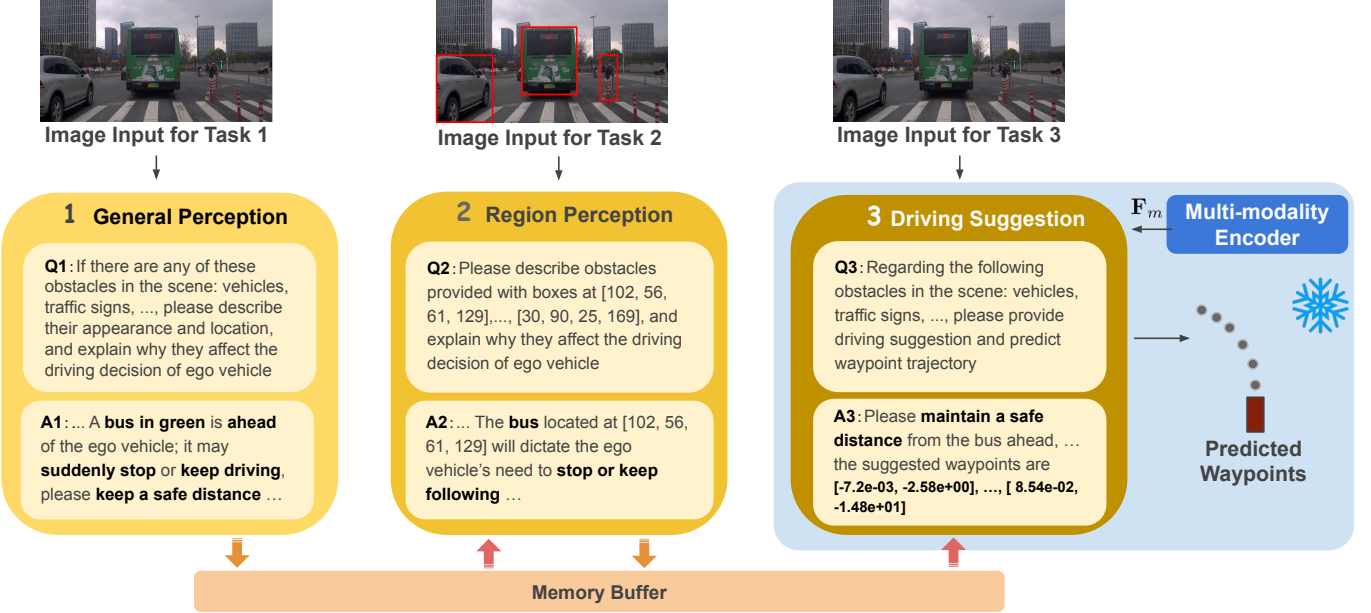


Fig. 5: The flow of VLM fine-tuned with CoT. The process formulates reasoning as a series of question-answer pairs in three tasks: General Perception, Region Perception, and Driving Suggestion. During the fine-tuning, the output of each task is saved into a memory buffer and further used for the following ones. The fine-tuned VLM is frozen during the end-to-end training and inference time of AppleVLM, which is demonstrated in the blue region.

and 3) *Driving Suggestion*, where the aim is to suggest a driving trajectory represented by a set of waypoints based on the results from previous tasks.

Fig. 5 illustrates the CoT process with an example. During the fine-tuning, the output answer of each task, as the chain, is concatenated in the prompt for the following tasks. By fine-tuning explicit tasks, the VLM hierarchically enriches its vision-language pairs, thereby enhancing its reasoning capabilities. Note that during the training and inference time of the end-to-end AppleVLM, we only adopt the last task of the CoT, *i.e.*, inputting the encoded feature \mathbf{F}_m and the question of *Driving Suggestion* to the VLM to generate the suggested driving waypoints. This significantly improves the computational efficiency of AppleVLM and allows it to run smoothly on constrained hardware platforms without requiring excessive computing resources, enabling real-time running in real-world deployment.

Control Model: Once the driving waypoints are predicted, we utilize a dynamic control model with the Linear Quadratic Regulator (LQR) algorithm [44] to output the control signals for driving: steering, throttle and brake.

C. Loss Function

The whole training process of AppleVLM consists of three stages and hence different loss functions are defined at different stages:

1) *Vision Encoder Pre-training with BEVs*: To enhance the spatial understanding of driving scenes, we pre-trained our vision encoder using BEV data covering three semantics: surrounding agents, lane boundaries, and drivable areas. The loss function consists of three parts.

Classification Loss: for classification of C_s categories, the focal loss \mathcal{L}_{cls} is defined as below:

$$\mathcal{L}_{cls} = - \sum_{c=1}^{C_s} \alpha_c (1 - p_c)^{\gamma_c} \log(p_c)$$

where p_c represents the predicted probability of category c ; α_c is the weight factor to alleviate the class imbalance; γ_c is the parameter of modulation factor $(1 - p_c)^{\gamma_c}$, which is used to control the contribution of classifying category c to the loss. A larger γ_c reduces the loss of categories with high p_c , forcing the model to pay more attention to the hard misclassified categories. In our case, we set $C_s = 7$, including categories of vehicle, pedestrian, red light, road lane, lane marking, sidewalk, and unlabeled, and we consider two hard-to-classify categories: pedestrian and lane marking.

Road Structure Loss: The cross-entropy loss is used for classifying the lane boundary and drivable area and background:

$$\mathcal{L}_{road} = - \frac{1}{N} \sum_{i=1}^N \sum_{c_d=1}^{C_d} y_{i,c_d} \log(p_{i,c_d})$$

where $C_d = 3$, p_{i,c_d} denotes the predicted probability of grid pixel i belonging to category c_d , and y_{i,c_d} is the ground truth.

Occupancy Loss: \mathcal{L}_{occ} is the binary focal loss applied on the BEV map for classifying background/foreground objects, defined as below:

$$\mathcal{L}_{occ} = \alpha_t (1 - p_t)^\gamma \log(p_t)$$

where p_t indicates the predicted probability of a pixel occupied by foreground objects, and the weight factor α_t and the parameter γ of modulation factor are adjusted to force the model to focus more on the foreground pixels.

2) *Planning Strategy Encoder Training*: Following the EP-SILON [39] method, we train the planning strategy encoder via imitation learning and freeze it during inference. Given a state sequence s_t , the objective is to minimize the negative log-likelihood of the action distribution of the policy with respect to expert demonstrations, described by:

$$\mathcal{L}_{PS} = - \sum_{t=1}^T \log \pi_\theta(a_t^{\text{expert}} \mid s_t), \quad (3)$$

where π_θ is the policy network and T is the trajectory length.

3) *VLM Fine-tuning with Corner Cases*: When fine-tuning the VLM decoder, we apply negative log-likelihood loss function \mathcal{L}_{NLL} as below:

$$\mathcal{L}_{\text{NLL}} = - \sum_{t=1}^T \log p(y_t \mid y_{<t}, x)$$

where $x = (x_1, x_2, \dots, x_T)$ is the input prompt tokens and $y = (y_1, y_2, \dots, y_T)$ is the target output sequence. For a sequence with the length of T , the goal of the model is to generate sequence $y_{<t} = (y_1, y_2, \dots, y_{T-1})$ that approximates to the target sequence y .

4) *End-to-end Training of AppleVLM*: Once we obtain the pre-trained vision encoder and the fine-tuned VLM decoder, we freeze these two modules and further train the AppleVLM for driving using an L_1 loss between the predicted waypoints and the ground truth waypoints. Let \mathbf{w}_k^* and \mathbf{w}_k^{gt} represent the predicted and ground truth waypoints at timestep k respectively, the loss function is defined as follows:

$$\mathcal{L}_{\text{drive}} = \frac{1}{K} \sum_{k=1}^K \|\mathbf{w}_k^* - \mathbf{w}_k^{gt}\|_1$$

IV. ENVIRONMENT

A. Driving on CARLA

1) *Dataset*: Our dataset is built upon the CARLA [45] 0.9.10. As mentioned in Sec. III-A, we adopt an expert agent (the same as [27]) in the CARLA environment to collect data along the routes defined in the Longest6 [30] and LangAuto [18] benchmarks. Further, we augment the dataset with the semantic topology model from [18] to generate natural language navigation data, and the planning method from [39] to generate planning corridor data. The corresponding BEVs are also collected following [27]. The whole dataset covers eight public towns in CARLA, with six towns (Town 1, 3, 4, 6, 7, 10) dedicated to training and two (Town 2, 5) for testing. It includes diverse driving scenarios with varied road structures, such as roundabouts, multi-lane highways, and complex intersections, and covers seven weather conditions (Clear, Cloudy, WetCloudy, SoftRain, MidRain, HardRain) and three daylight conditions (Noon, Night, Sunset).

Regarding the onboard sensors, we set up one LiDAR sensor, and four RGB cameras pointing to the front, left, right, and rear. The front camera is located at $(x : 1.3, y : 0.0, z : 2.3)$ with a yaw angle of 0° , while the two side cameras are with the same location but angled at -60° and 60° , respectively. The rear camera is placed at $(x : -1.3, y : 0.0, z : 2.3)$ and

angled at 180° . Each of the cameras outputs images with a resolution of 960×480 pixels, covering horizontal field of view (HFOV) of 120° .

2) *Metrics*: We conduct the driving testing for models on two CARLA benchmarks, LangAuto [18] and Longest6 [30]. In each benchmark, a set of driving routes with specific settings is pre-defined. The driving agents are rolled out in the environment and evaluated the driving performance with metrics. For each driving route, we measure the driving performance of the agents with three metrics defined by CARLA Leaderboard [45]: the driving score (DS), route completion (RC), and infraction score (IS), described below:

$$\begin{cases} RC = \frac{L_{\text{completed}}}{L_{\text{total}}} \\ IS = IS_0 \times \prod_{n=1}^N \delta_n \\ DS = RC \times IS \end{cases} \quad (4)$$

where L_{total} and $L_{\text{completed}}$ are the total route length, and the completed route length, respectively. RC represents the percentage of the route distance completed by an agent; IS measures the traffic rule violations, where IS_0 is the initial driving score. Regarding the occurred violation, IS_0 is multiplied by the corresponding factor δ_n , and the scores of N violations are summed up; DS is the product of the RC and the IS .

By default setting of the CARLA Leaderboard, only a timeout or a deviation from the route can trigger the termination of the episode. We propose a new metric RC_{strict} ,

$$RC_{\text{strict}} = \frac{L_s}{L_{\text{total}}}.$$

where L_s denotes the route distance completed by the agent under zero tolerance for any traffic infraction, such as failing to stop at a red traffic light or colliding with vehicles/pedestrians. The metric RC_{strict} reflects a higher restriction on driving safety.

We also use M_{prec} to measure the precision of the BEVs prediction. As defined below, the function in $GIOU(\cdot)$ computes the discrepancy of the predicted semantic BEVs, $\hat{\mathbf{B}}$ with ground-truth semantic BEVs, \mathbf{B} :

$$M_{\text{prec}} = GIOU(\hat{\mathbf{B}}, \mathbf{Y}) = \frac{|\hat{\mathbf{B}} \cap \mathbf{B}|}{|\hat{\mathbf{B}} \cup \mathbf{B}|} - \frac{|\mathbf{C} \setminus (\hat{\mathbf{B}} \cup \mathbf{B})|}{|\mathbf{C}|},$$

where \mathbf{C} is the area of the smallest enclosing convex shape in prediction and ground truth.

B. VLM Fine-tuning with Corner Cases

1) *Datasets*: We adopt the corner-case dataset CODA-LM [43] and DriveLM [35] to fine-tune the VLM backbone of AppleVLM. CODA-LM comprises 9,768 real-world driving scenarios (images), each attached with one question-answer (QA) pair generated by ChatGPT. In contrast, DriveLM introduces spatial-temporal reasoning with graph-structured VQAs from both nuScenes (4,871 frames) and CARLA (183,000 frames), covering sub-tasks of perception, prediction, and planning. To enable joint training by these two datasets, we

TABLE I: Performance comparison of 8 end-to-end driving models on the LangAuto [18] benchmark. The \uparrow stands for the higher the better. For each metric, the best result is shown in bold.

Model	Cond.	LangAuto				LangAuto Short				LangAuto Tiny				
		$DS \uparrow$	$RC \uparrow$	$RC_{strict} \uparrow$	$IS \uparrow$	$DS \uparrow$	$RC \uparrow$	$RC_{strict} \uparrow$	$IS \uparrow$	$DS \uparrow$	$RC \uparrow$	$RC_{strict} \uparrow$	$IS \uparrow$	
TCP [29]	TP	39.1 ± 0.9	73.5 ± 2.2	20.4 ± 2.2	0.46 ± 0.06	47.6 ± 4.2	78.1 ± 3.1	28.7 ± 3.1	0.61 ± 0.03	50.7 ± 1.2	89.1 ± 4.3	33.1 ± 4.3	0.57 ± 0.06	
Transfuser [27]	TP	37.0 ± 3.1	74.0 ± 3.5	14.9 ± 3.5	0.50 ± 0.06	41.4 ± 1.1	81.2 ± 2.6	20.1 ± 2.6	0.51 ± 0.03	47.2 ± 1.2	93.0 ± 5.0	29.1 ± 5.0	0.50 ± 0.06	
Transfuser++ [21]	TP	58.7 ± 1.1	82.1 ± 2.5	56.2 ± 3.0	0.71 ± 0.02	64.8 ± 1.9	85.2 ± 2.3	63.8 ± 1.5	0.76 ± 0.04	75.3 ± 2.2	95.5 ± 2.3	74.1 ± 1.2	0.81 ± 0.02	
UniAD [4]	NC	40.4 ± 1.8	80.0 ± 2.9	36.1 ± 2.9	0.51 ± 0.04	40.2 ± 2.4	83.1 ± 4.4	36.9 ± 4.4	0.61 ± 0.02	47.1 ± 4.1	89.1 ± 1.1	37.1 ± 1.1	0.75 ± 0.03	
Interfuser [28]	NC	36.7 ± 0.7	72.1 ± 4.1	26.7 ± 4.1	0.51 ± 0.06	44.6 ± 3.1	74.4 ± 4.6	30.2 ± 4.6	0.60 ± 0.08	48.1 ± 3.0	74.5 ± 5.0	35.2 ± 5.0	0.65 ± 0.05	
LMDrive [18]	NC	36.2 ± 2.3	46.5 ± 4.3	41.1 ± 4.3	0.81 ± 0.03	50.6 ± 1.7	60.0 ± 3.4	50.6 ± 1.7	0.84 ± 0.04	66.5 ± 3.6	77.9 ± 2.3	54.8 ± 2.3	0.85 ± 0.02	
AppleVLM	LLaVA	NC	52.5 ± 1.5	63.2 ± 1.3	56.2 ± 1.5	0.83 ± 0.04	59.9 ± 1.1	71.3 ± 1.5	57.3 ± 1.4	0.84 ± 0.02	67.2 ± 1.6	78.1 ± 1.2	68.7 ± 1.1	0.86 ± 0.02
	Janus Pro	NC	59.2 ± 1.9	67.1 ± 3.4	59.1 ± 3.1	0.89 ± 0.04	66.0 ± 1.6	76.9 ± 3.7	64.5 ± 3.9	0.91 ± 0.03	76.0 ± 3.3	83.5 ± 2.0	76.9 ± 1.9	0.91 ± 0.02

TABLE II: Performance comparison of 8 end-to-end driving models on Longest6 [30] benchmark. The \uparrow stands for the higher the better. For each metric, the best result is shown in bold.

Model	Cond.	$DS \uparrow$	$RC \uparrow$	$RC_{strict} \uparrow$	$IS \uparrow$
TCP [29]	TP	32.5 ± 0.9	81.2 ± 1.2	17.2 ± 2.2	0.40 ± 0.05
Transfuser [27]	TP	38.6 ± 0.9	84.1 ± 1.2	15.3 ± 3.5	0.42 ± 0.06
Transfuser++ [21]	TP	62.3 ± 1.1	89.0 ± 1.0	59.2 ± 3.2	0.70 ± 0.01
UniAD [4]	NC	38.1 ± 1.8	79.9 ± 1.7	34.2 ± 2.9	0.46 ± 0.06
Interfuser [28]	NC	45.4 ± 0.9	88.9 ± 5.3	18.9 ± 4.1	0.51 ± 0.06
LMDrive [18]	NC	35.8 ± 2.3	43.1 ± 2.5	38.1 ± 4.3	0.83 ± 0.03
AppleVLM	LLaVA	NC	53.4 ± 3.1	62.1 ± 2.7	54.2 ± 4.3
	Janus Pro	NC	60.5 ± 2.1	68.7 ± 3.7	60.9 ± 1.2
					0.88 ± 0.02

annotated the DriveLM following the QA-pair format used in the CODA-LM to align data formats. For more details please refer to [43] and [35].

2) *Metrics*: For CODA-LM, we follow its benchmark [43] and report performance using the Text-Score (TS) of correctness from GPT-4, normalized to [1, 100]. For three tasks of CoT, we compute the TS_{gp} , TS_{tp} , and TS_{ds} , and provide the TS_{avg} (the average of the three TS) in Tab. VI. For DriveLM, evaluation relies on *SPICE*, *GPT Score*, and *Completeness* metrics. *SPICE* converts predictions and ground truth into scene graphs and computes the *F-score*. *GPT Score* is a reasoning-based score from 0 to 100 judged by GPT-4. *Completeness* measures the fraction of QAs correctly answered above a given threshold.

V. EXPERIMENTS

A. Experimental Setup

1) *Training Details*: We took RegNet64 [46] as the backbone to process the RGB images and LiDAR point-cloud data in the vision encoder and Janus Pro [42] as the backbone of our VLM decoder. All three stages of training were with the AdamW optimizer [47]. When pre-training the vision encoder with BEV maps, we used an initial learning rate (LR) of $5e^{-5}$ and weight decay of 0.01. We trained the model for 50 epochs on one NVIDIA 4090 GPU, with a batch size of 64. The LR was scheduled with cosine annealing [48], which dynamically adjusted LR in the shape of a cosine curve until the minimum LR=0. During the fine-tuning of the VLM decoder, we set an initial learning rate of $2e^{-5}$ and weight decay of 0.05. The model was trained for 12 epochs on 10 NVIDIA A6000 GPUs in parallel, with a batch size of 12. The LR decays following cosine annealing. To train the end-to-end AppleVLM, we used

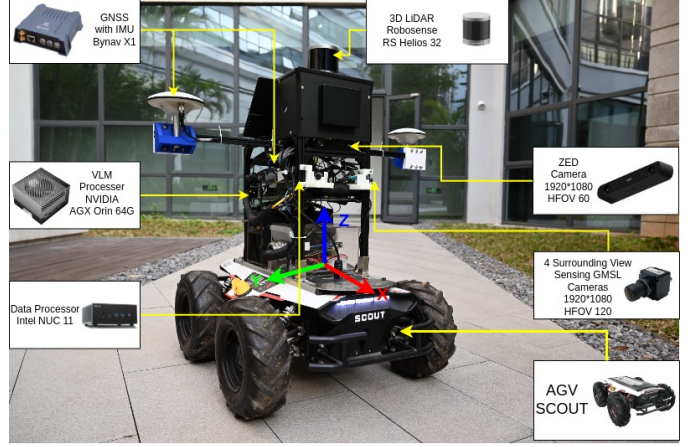


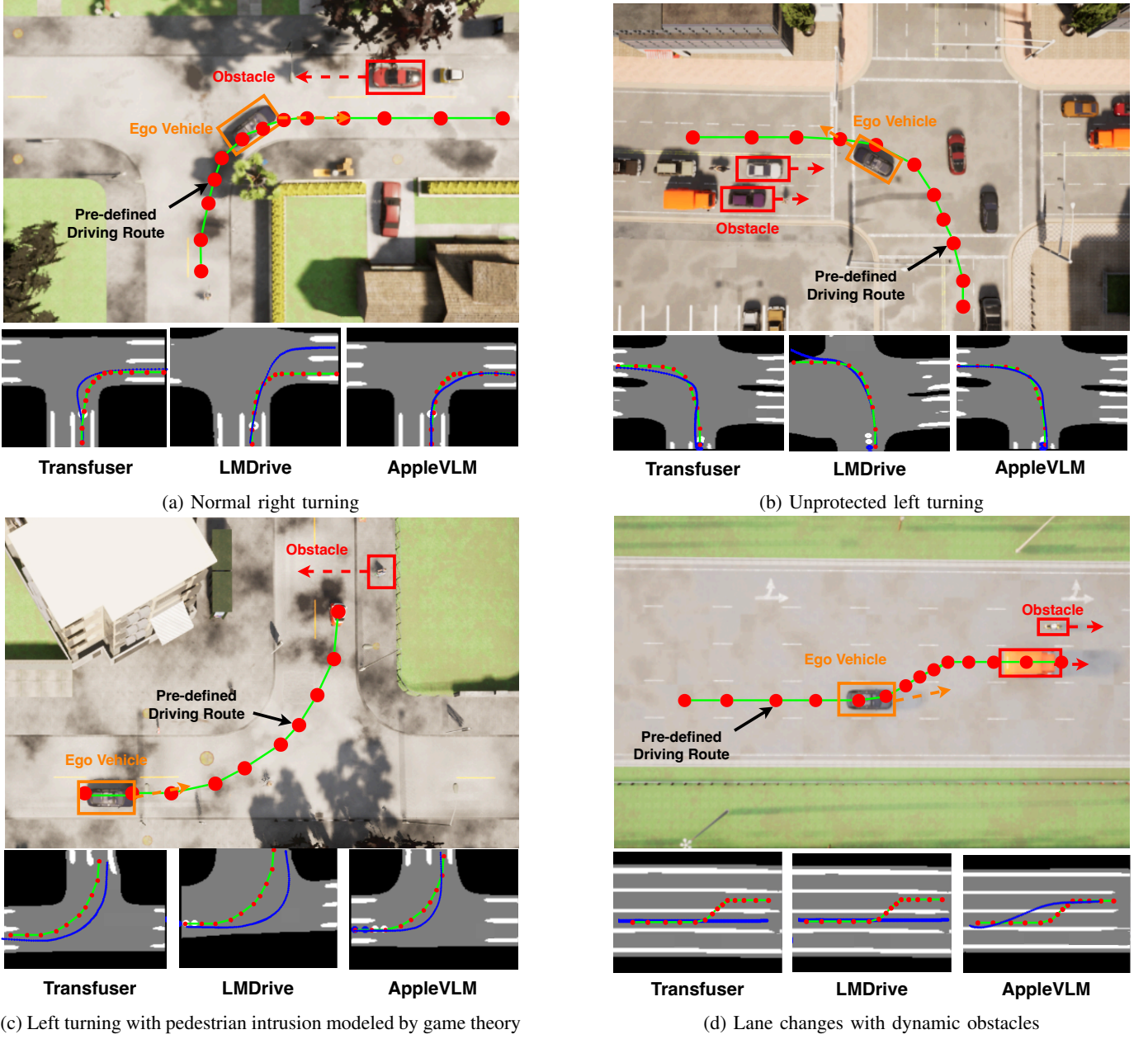
Fig. 6: AGV platform for real-world deployment

an initial learning rate of $1e^{-5}$ and weight decay of 0.01. We trained it for 10 epochs on 10 NVIDIA A6000 GPUs in parallel, with a batch size of 8. The learning rate linearly decayed with warm-up in the first 5% of the training steps.

2) *Real-world Deployment*: We deployed the learned end-to-end driving policy of AppleVLM on a Scout automated guided vehicle(AGV) platform. As depicted in Fig. 6, the AGV was equipped with an NVIDIA Jetson AGX Orin with 64GB SOC processor for VLM process and Intel NUC 11 for data process. The sensor suite consisted of a Bynav X1 GNSS and IMU for approximate localization and pose, a Robosense RS Helios 32 LiDAR sensor, one ZED camera with 60° HFOV at resolution of 1920×1080 , and four Sensing SG2-GMSL cameras with 120° HFOV at resolution of 1920×1080 pixels for capturing visual observations. The navigation instruction and global navigation information came from Amap navigation SDK.

B. CARLA Experiments

The experiments on the CARLA simulator consist of four parts. Firstly, we perform the driving test for all models on two public benchmarks (LangAuto [18] and Longest6 [27]) to provide quantitative results and analysis. Then, for intuitive comparison, we qualitatively evaluate the model's performance in four specific scenarios defined in our study: normal right turn, unprotected left turn, unprotected left turn with pedestrian intrusions modeled by game theory, and lane change with dynamic obstacles. Next, we compare the influence of changes in sensor settings and show the robustness of AppleVLM.



(c) Left turning with pedestrian intrusion modeled by game theory

(d) Lane changes with dynamic obstacles

Fig. 7: Qualitative results of Transfuser, LMDrive, and AppleVLM in four specific driving scenarios. The driving trajectories are completed in a closed-loop driving environment on the CARLA simulator. In each sub-figure, we show on top the driving scenario from a bird's eye view. The orange block along with a pointer indicates the ego vehicle and its driving direction. The red dotted line represents the dynamic obstacles that potentially affect the ego vehicle, and the pointer points to its driving direction. At the bottom, we show the predicted BEVs with driving trajectories. The green lines with red dots indicate the pre-defined driving trajectories, and the blue ones are the actual driving trajectories.

Finally, we conduct an ablation study on key parts of the AppleVLM.

1) *Quantitative Results*: In Tab. I and II, we summarize the quantitative results of different methods tested on LangAuto and Longest6 benchmarks. For comparison, we select five typical uni-modal end-to-end driving models that are solely based on vision: Transfuser [27], Interfuser [28], TCP [29], UniAD [4] and Transfuser++ [21]. Since there are few existing VLM-based driving models, we only consider the latest proposed LMdrive [18], along with two AppleVLM models

embedded with the LLaVA v1.5 [49] and Janus Pro [42] backbones, fine-tuned with both CODA-LM and DriveLM datasets. As introduced in Transfuser++ [21], in the table, we use *TP* (map-based GNSS localization of the target points) and *NC* (discrete commands *e.g.*, follow lane, turn right) to indicate models that receive navigation information based on two different conditions (Cond.). Considering the variance in different training runs, we use 3 different random seeds for the training of each method. For each method, we select the model with the best offline evaluation results (*i.e.*, the lowest

TABLE III: The influence of changes in sensor configuration for all models. The models are tested on LangAuto [18] benchmark. The \uparrow stands for the higher the better.

Setting	Transfuser				LMDrive				AppleVLM w/o $\mathcal{D}\mathcal{A}$				AppleVLM with $\mathcal{D}\mathcal{A}$			
	$M_{\text{prec}} \uparrow$	Gain	$RC \uparrow$	Gain	$M_{\text{prec}} \uparrow$	Gain	$RC \uparrow$	Gain	$M_{\text{prec}} \uparrow$	Gain	$RC \uparrow$	Gain	$M_{\text{prec}} \uparrow$	Gain	$RC \uparrow$	Gain
Original	69.11	-	74.0 ± 3.5	-	63.27	-	46.5 ± 4.3	-	67.23	-	59.9 ± 1.7	-	71.12	-	67.1 ± 3.4	-
1	47.11	-22.00	21.5 ± 4.3	-52.5	43.56	-19.71	23.0 ± 3.5	-23.5	53.96	-13.27	54.2 ± 3.1	-5.7	60.55	-10.57	63.6 ± 3.9	-3.5
2	31.02	-38.09	17.3 ± 1.7	-56.7	34.70	-28.57	18.7 ± 3.2	-27.8	50.73	-16.50	47.6 ± 2.5	-12.3	57.12	-14.00	58.2 ± 3.7	-8.9
3	28.21	-38.09	15.2 ± 2.3	-58.8	34.10	-29.17	15.8 ± 2.9	-30.7	45.52	-21.71	44.1 ± 2.3	-15.8	53.09	-18.03	55.6 ± 3.2	-11.5
4	27.33	-41.78	27.2 ± 2.9	-46.8	30.94	-32.33	14.4 ± 0.5	-32.1	42.78	-24.45	51.6 ± 2.9	-8.3	52.17	-18.95	63.0 ± 1.4	-4.1
5	51.55	-17.56	13.4 ± 1.5	-60.6	44.98	-18.29	21.0 ± 1.7	-25.5	50.10	-17.13	38.4 ± 1.3	-21.5	54.51	-16.61	51.4 ± 0.6	-15.7

Note: Parameters different from the original setting are shown in **bold**:

Setting	Front		Left		Right	
	Position	Rotation	Position	Rotation	Position	Rotation
Original	$(1.3, 0.0, 2.3)$	$(0^\circ, 0^\circ, 0^\circ)$	$(1.3, 0.0, 2.3)$	$(0^\circ, 0^\circ, -60^\circ)$	$(1.3, 0.0, 2.3)$	$(0^\circ, 0^\circ, 60^\circ)$
1	$(1.3, 0.0, 2.3)$	$(0^\circ, 0^\circ, 0^\circ)$	$(1.3, 0.0, 2.3)$	$(0^\circ, 0^\circ, -90^\circ)$	$(1.3, 0.0, 2.3)$	$(0^\circ, 0^\circ, 90^\circ)$
2	$(1.3, 0.0, 2.3)$	$(0^\circ, 0^\circ, 0^\circ)$	$(\mathbf{1.3, 0.5, 2.3})$	$(0^\circ, 0^\circ, -90^\circ)$	$(\mathbf{1.3, 0.5, 2.3})$	$(0^\circ, 0^\circ, 90^\circ)$
3	$(\mathbf{0.8, 0.0, 2.3})$	$(0^\circ, 0^\circ, 0^\circ)$	$(1.3, 0.0, 2.3)$	$(0^\circ, 0^\circ, -60^\circ)$	$(1.3, 0.0, 2.3)$	$(0^\circ, 0^\circ, 60^\circ)$
4	$(1.3, 0.0, 2.3)$	$(0^\circ, -30^\circ, 0^\circ)$	$(1.3, 0.0, 2.3)$	$(0^\circ, 0^\circ, -60^\circ)$	$(1.3, 0.0, 2.3)$	$(0^\circ, 0^\circ, 60^\circ)$
5	$(1.3, 0.0, 2.3)$	$(\mathbf{30^\circ, 0^\circ, 0^\circ})$	$(1.3, 0.0, 2.3)$	$(0^\circ, 0^\circ, -60^\circ)$	$(1.3, 0.0, 2.3)$	$(0^\circ, 0^\circ, 60^\circ)$

mean absolute error) and further perform the driving test on CARLA benchmarks. To account for the non-determinism of closed-loop driving on CARLA, we repeat the driving test of each model 3 times and report their mean and standard deviation in the table.

It can be found from Tab. I that the proposed AppleVLM achieves the best performance in both *DS* and *IS* among three sub-tasks of the LangAuto benchmark. Although the *TP* conditioned TransFuser++ outperforms AppleVLM in *RC*, it conditions predictions using the next target point along the route, which tends to be more easily recover from steering errors (proved in [21]); in contrast, AppleVLM only uses the discrete navigation commands that contain no geometric information about the center of the lanes. Compared to the latest proposed VLM-based method LMDrive, AppleVLM improves *RC* by 16.7 and 20.6 in long-distance driving (longer than 500 meters). In two short-distance driving tasks that contain routes less than 500 meters, AppleVLM still maintains the best performance, leading by 11.3 and 16.9 in LangAuto short, while 0.2 and 5.6 in LangAuto Tiny, respectively.

Compared to the vision-based models, the VLM-based models generally obtain lower *RC* results. We observe that this is because in the original benchmark setting, an episode is not terminated when a collision occurs unless the ego vehicle deviates from the desired lane. Inspired by [26], we propose the RC_{strict} metric, where an episode is terminated and counted as failed once any traffic violation occurs (including collision, route deviation *etc.*). In this case, we find that the vision-based models have a significant decline in completing the route driving, and all the VLM-based models can achieve better results than the vision-based models. AppleVLM with fine-tuned Janus pro achieves the best RC_{strict} results among all models with the lead of 18.0, 13.9 and 22.1 compared to the LMDrive, and 2.9, 0.7 and 2.8 to the Transfuser++. Moreover, we can find that the results of Longest6 (Tab. II) demonstrate the same conclusion as LangAuto, which further shows the remarkable advantage of AppleVLM over other models.

2) *Qualitative Analysis*: Fig. 7 shows the driving trajectories of the vision-based driving model Transfuser and

the VLM-based driving model LMDrive, and the proposed AppleVLM across four specific scenarios, depicted in a BEV format. In general, AppleVLM consistently generates driving trajectories that most closely align with the desired ones in all scenarios. Specifically, LMDrive is prone to deviating from the driving lane (either driving into the opposite lane or the sidewalk) when turning (see Fig. 7a and 7b). Transfuser can mostly complete the turning but tends to drift unnecessarily (see Fig. 7a and 7b). When a lane change is required, only AppleVLM can respond effectively and make a reasonable lane change in the presence of other vehicles (see Fig. 7d).

3) *Robust to Sensor Configuration Changes*: To examine the robustness of AppleVLM to the sensor change, we conduct experiments using Transfuser, LMDrive and AppleVLM without $\mathcal{D}\mathcal{A}$ as the comparative models. We alter the position (x, y, z) and rotation (roll, pitch, yaw) of three cameras and make 5 sensor settings different from the original setting during data collection, as detailed in Tab. III. The comparison experiments are conducted on the LangAuto benchmark. We use *RC* as the metric to reflect the driving performance. In addition, we provide M_{prec} of BEV prediction, which roughly reflects the interpretability of the visual encoder, as a reference.

Comparing AppleVLM to Transfuser and LMDrive, we see that under setting 1 and 2, Transfuser is extremely sensitive to the change in two side cameras, which is reflected in the rapid decline of -52.5 and -56.7 in *RC*. LMDrive performs slightly better than Transfuser, with only half of the performance drop (-23.5 and -27.8 in *RC*). In contrast, the AppleVLM is more robust with only slight decreases of -3.5 and -8.9 . A similar trend is observed in the prediction of BEVs, where AppleVLM outperforms Transfuser and LMDrive with the smaller decrease in M_{prec} results. All models are affected by the position change in the front camera (setting 3), while the Transfuser and LMDrive exhibit a dramatic performance decline in two metrics (-38.09 and -58.8 , -29.17 and -30.7) compared to AppleVLM (-18.03 and -11.5). When adjusting the pitch of the front camera to -30° (setting 4), the *RC* results of Transfuser and LMDrive decreased by 46.8 and 32.1 respectively, approximately 10 and 8 times the decline

TABLE IV: Ablation study on the impact of vision encoder design. The models are tested on LangAuto [18] benchmark. The \uparrow stands for the higher the better. For each metric, the best result is shown in bold.

Vision Encoder	$M_{\text{precision}} \uparrow$	$DS \uparrow$	$RC \uparrow$	$IS \uparrow$
LMDrive [18]	47.23	29.8 ± 2.3	46.5 ± 4.3	0.64 ± 0.03
Transfuser [27]	69.11	33.1 ± 3.1	51.0 ± 3.5	0.66 ± 0.06
BEVformer [50]	57.82	37.6 ± 1.5	53.0 ± 4.3	0.71 ± 0.03
ResNet-50	59.91	42.5 ± 1.8	55.3 ± 3.0	0.75 ± 0.01
AppleVLM	RegNet-32	65.79	48.6 ± 1.1	60.1 ± 1.2
AppleVLM	RegNet-64	71.12	52.6 ± 2.2	65.5 ± 5.3
				0.88 ± 0.04

TABLE V: Ablation study on the impact of planning strategy encoder. The models are tested on LangAuto [18] benchmark. The \uparrow stands for the higher the better. For each metric, the best result is shown in bold.

Model		$DS \uparrow$	$RC \uparrow$	$IS \uparrow$
LLaVA v1.5	w/o \mathcal{T}_P	36.2 ± 2.3	46.5 ± 4.3	0.81 ± 0.03
	w/ \mathcal{T}_P	44.6 ± 1.1	57.2 ± 5.3	0.78 ± 0.01
Janus Pro	w/o \mathcal{T}_P	40.4 ± 1.7	50.5 ± 1.6	0.80 ± 0.03
	w/ \mathcal{T}_P	48.7 ± 2.3	60.1 ± 3.1	0.81 ± 0.02
Fine-tuned Janus Pro	w/o \mathcal{T}_P	44.1 ± 2.2	51.1 ± 5.3	0.88 ± 0.04
	w/ \mathcal{T}_P	52.6 ± 2.2	65.5 ± 5.3	0.88 ± 0.04

observed in AppleVLM; and the BEV prediction performance of all models declined, with Transfuser exhibiting a dramatic drop of -41.78 . A similar trend is observed in setting 5, when changing the roll to 30° , the RC of Transfuser is significantly reduced by 60.6, which is almost 5 times the decline of AppleVLM. Although LMDrive performs more stably than Transfuser under this setting, it still drops nearly 10 points more than AppleVLM. Notably, through comparative experiments on whether to apply \mathcal{DA} to AppleVLM, we observe that for all sensor changes, AppleVLM with \mathcal{DA} consistently exhibits less decline in both M_{prec} and RC metrics. This demonstrates that \mathcal{DA} plays a crucial role in helping AppleVLM to maintain more stable performance when sensor conditions change.

4) *Ablation Study*: In the ablation study, we are interested in the impact of several key parts of AppleVLM: the proposed novel vision encoder, the planning strategy encoder for multi-modal feature fusion, and the corner-case fine-tuning for the VLM backbone.

Vision Encoder: We replace our proposed vision encoder in AppleVLM with the ones from LMDrive [18], Transfuser [27], and BEVformer [50] respectively to verify its efficiency. In Tab. IV, we provide results of $M_{\text{precision}}$ that reflect on the lane perception and DS , RC and IS that indicate the driving performance. The results illustrate that AppleVLM embedded with our proposed vision encoder achieves the highest scores in all metrics, whereas the one with the ResNet-64 backbone yields the best performance. Meanwhile, changing the ResNet backbone might slightly alter the driving results, while all of them are superior to the above models. This fully reveals the effectiveness of our vision encoder based on the deformable attention.

Planning-enhanced VLM: As described in Fig. 4, compared

TABLE VI: Ablation study on the impact of corner-case fine-tuning for text prediction of VLMs. The models are tested on the CODA-LM [43] benchmark. The \uparrow stands for the higher the better. For each metric, the best result is shown in bold.

VLM backbone	Model	$TS_{\text{gp}} \uparrow$	$TS_{\text{rp}} \uparrow$	$TS_{\text{ds}} \uparrow$	$TS_{\text{avg}} \uparrow$
LLaVA v1.5 Baseline	-	28.17	19.30	42.06	23.16
Fine-tuned LLaVA v1.5	NexusAD [51]	68.97	57.58	84.31	65.02
Fine-tuned LLaVA v1.5	Ilmforad [52]	72.12	58.70	83.41	74.26
Janus Pro Baseline	-	25.88	52.06	30.90	36.28
Fine-tuned Janus Pro	AppleVLM	73.14	59.11	85.11	75.12

to the traditional VLMs, AppleVLM incorporates a planning strategy encoder module, aiming to enhance the feature extraction and fusion for better driving performance. To verify this, we conduct three sets of comparative experiments: the vanilla LLaVA v1.5, the vanilla Janus Pro, and the fine-tuned Janus Pro, all with and without a planning strategy encoder module. The driving results on the LangAuto benchmark are summarized in Tab. V. In general, incorporating the planning features into the Q-former feature fusion improves DS and RC results for all models, where the fine-tuned Janus Pro one shows the most significant increase (+8.5 and +14.4). During the driving tests, we observe that when the driving model receives navigation commands in the form of natural language, it often understands the navigation language commands incorrectly and hence responds incorrectly, resulting in the ego vehicle deviating from the desired driving route. An example is shown in Fig. 7(d). The planning strategy encoder provides explicit spatial information for navigation, thus incorporating it facilitates feature fusion of the vision and language modalities. To further explore how language input and the Planning Strategy Encoder (PSE) affect the model performance of following instructions, in Fig. 8, we provide a scenario in which the ego vehicle passes by an intersection and drives into a multi-lane road under different conditions: a basic or more precise navigation command, with or without PSE. The results reveal that the navigation ambiguity arises from language interpretation, while PSE can effectively solve the lane-oscillation problem, leveraging the explicit spatial information from planning tokens.

VLM Fine-tuned with Corner Cases: As described in Sec. III-A, the VLM backbone of AppleVLM is pre-trained with a real-world corner-case dataset before the last-stage end-to-end training. Our intuition is that the model can better generalize in long-tail scenarios by incorporating prior knowledge of corner cases. To verify the conjecture, we conduct comparison experiments on CODA-LM [43] and DriveLM [35] benchmarks.

Regarding CODA-LM, we consider LLaVA v1.5 [49] and Janus Pro [42], as well as two models that are fine-tuned on the LLaVA v1.5, NexusAD [51], Ilmforad [52] and our proposed AppleVLM that is fine-tuned on Janus Pro. For a comprehensive analysis, we first use the Text-Score metric TS to evaluate the standalone VLMs in three tasks of CoT (Tab. VI) among all models, and then compare the closed-loop driving performance of AppleVLM embedded with the vanilla or fine-tuned Janus Pro VLM backbone (Tab. VIII). It can be found from Tab. VI that in general, all the models fine-tuned

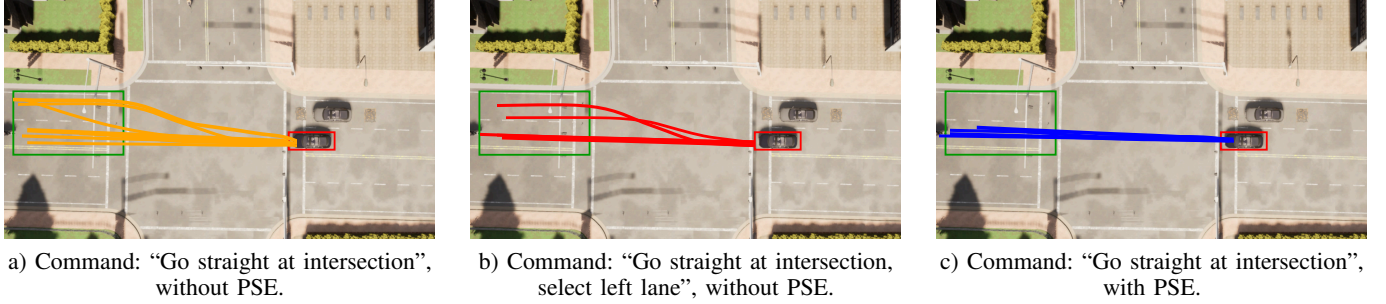


Fig. 8: Qualitative analysis of the effectiveness of the planning strategy encoder in eliminating lane oscillations when transitioning from an intersection to a multi-lane road. Each condition was evaluated over 10 runs.

TABLE VII: The experiments of models conducted on the DriveLM [35] benchmark. The \uparrow stands for the higher the better. For each metric, the best result is shown in bold.

VLM Model	SPICE \uparrow	GPT Score \uparrow	Completeness \uparrow
BLIP-2	4.336	42.97	1.064
DriveLM-agent	42.56	71.39	30.04
LLaVA v1.5 Baseline	31.85	53.51	21.43
Janus Pro Baseline	38.39	62.15	27.02
AppleVLM	45.45	72.04	31.15

with corner cases (*i.e.*, NexusAD, llmforad, and AppleVLM) significantly outperform the baselines without fine-tuning in text prediction among three CoT tasks. AppleVLM achieves the best TP results of 73.14, 59.11 and 85.11 in all three tasks, showing the highest gains (+47.26 and +54.21) in TP_{gp} and TP_{ds} after fine-tuning. This demonstrates that incorporating extreme scenarios in training can enhance the ability of VLMs to understand driving scenes.

On DriveLM benchmark, we consider two VLM baselines (BLIP2 and DriveLM-agent) that provided by [35]. As shown in Tab. VII, AppleVLM significantly outperforms BLIP-2 and DriveLM-agent on SPICE, GPT Score, and Completeness metrics, achieving the best results of 45.45, 72.04, and 31.15. Besides, AppleVLM surpasses the vanilla Janus Pro by +7.06, +9.89, and +4.13, respectively. These results demonstrate that the AppleVLM incorporating the CoT mechanism can effectively improve its spatial-temporal understanding capability.

We further explore the impact of CoT fine-tuning on the final closed-loop driving performance. We provide three settings of two VLM backbones (LLaVA v1.5 and Janus Pro): VLM baselines without fine-tuning, VLMs fine-tuned without CoT (*i.e.*, simply outputting driving suggestions), and VLMs fine-tuned with CoT. As shown in Tab. VIII, we see that fine-tuning VLMs is effective in improving end-to-end driving. Whether using LLaVA v1.5 or Janus Pro, CoT-based fine-tuning consistently outperforms simple-task fine-tuning, demonstrating the clear advantage of incorporating the CoT mechanism during the fine-tuning process.

CoT fine-tuning datasets: In Tab. IX, we analyze the impact of different datasets used for CoT fine-tuning of the VLM backbones on the final driving performance. We observe that either CODA-LM and DriveLM CoT fine-tuning for both LLaVA v1.5 and Janus Pro VLMs has a positive contribution

TABLE VIII: Ablation study on the impact of CoT fine-tuning for the final driving performance. The models are fine-tuned with both the DriveLM [35] and CODA-LM [43] datasets. The \uparrow stands for the higher the better. For each metric, the best result is shown in bold.

Backbone	CoT	$DS \uparrow$	$RC \uparrow$	$IS \uparrow$
LLaVA v1.5 Baseline	-	44.6 ± 1.1	57.2 ± 5.3	0.78 ± 0.01
Fine-tuned LLaVA v1.5	w/o	49.9 ± 1.7	60.9 ± 2.2	0.82 ± 0.06
Fine-tuned LLaVA v1.5	w/	52.5 ± 1.5	63.2 ± 1.3	0.83 ± 0.04
Janus Pro Baseline	-	48.7 ± 2.3	60.1 ± 3.1	0.81 ± 0.02
Fine-tuned Janus Pro	w/o	52.3 ± 2.1	61.5 ± 4.3	0.85 ± 0.03
Fine-tuned Janus Pro	w/	59.2 ± 1.9	67.1 ± 3.4	0.89 ± 0.04

TABLE IX: Ablation study on the impact of different datasets applied in CoT fine-tuning for VLMs driving performance. The \uparrow stands for the higher the better. For each metric, the best result is shown in bold.

Backbone	CODA-LM	DriveLM	$DS \uparrow$	$RC \uparrow$	$IS \uparrow$
LLaVA v1.5	-	-	44.6 ± 1.1	57.2 ± 5.3	0.78 ± 0.01
LLaVA v1.5	✓	-	50.4 ± 1.5	61.5 ± 1.7	0.82 ± 0.04
LLaVA v1.5	-	✓	51.4 ± 1.6	62.7 ± 1.9	0.82 ± 0.04
LLaVA v1.5	✓	✓	52.5 ± 1.5	63.2 ± 1.3	0.83 ± 0.04
Janus Pro	-	-	48.7 ± 2.3	60.1 ± 4.5	0.81 ± 0.02
Janus Pro	✓	-	55.0 ± 2.2	63.5 ± 5.3	0.88 ± 0.04
Janus Pro	-	✓	56.6 ± 1.7	65.5 ± 3.1	0.88 ± 0.04
Janus Pro	✓	✓	59.2 ± 1.9	67.1 ± 3.4	0.89 ± 0.04

to improve the model’s driving performance. Compared to CODA-LM, DriveLM yields a slight advantage in performance gain. The best results are achieved when using both datasets.

Freezing Vision Encoder: As shown in Tab. X, we study the impact of freezing or fine-tuning vision encoder in the training process of driving task. We observe that fine-tuning the visual encoder yields only marginal gains (+1.8 in RC and +1.0 in DS), yet prolongs training time and increases the number of trainable parameters by 5 times per epoch. To strike a balance between performance and efficiency, in this work, we freeze the pre-trained vision encoder when training the driving task.

Input Modality: As shown in Tab. XI, we analyze the impact of different modalities on the model driving performance, evaluated on the LangAuto benchmark. We see that incorporating all the vision, language, and planning modules contributes to the best driving performance of AppleVLM. Removing

TABLE X: Ablation study on the impact of freezing or fine-tuning the vision encoder. The models are tested on LangAuto [18] benchmark. The \uparrow stands for the higher the better. The best result is shown in bold.

Vision Encoder Status	<i>DS</i> \uparrow	<i>RC</i> \uparrow	<i>IS</i> \uparrow	Trainable Params (M)	Training Time (h/epoch)
freezing	60.5 ± 2.1	68.7 ± 3.7	0.88 ± 0.02	23	6.5
jointly fine-tuning	61.5 ± 1.8	70.5 ± 2.6	0.88 ± 0.01	127	9

TABLE XI: Ablation study on the contributions of different modalities to end-to-end autonomous driving performance. The models are evaluated on the LangAuto [18] benchmark. \uparrow indicates higher is better. For each metric, the best result is shown in bold.

Input Modality				Performance		
Image	LiDAR	BEV tokens	Language	<i>DS</i> \uparrow	<i>RC</i> \uparrow	<i>IS</i> \uparrow
✓	✓	✓	✓	59.2 ± 1.9	67.1 ± 3.4	0.89 ± 0.04
✓		✓	✓	33.6 ± 1.8	55.1 ± 1.3	0.61 ± 0.04
	✓	✓	✓	29.8 ± 1.9	52.2 ± 2.1	0.57 ± 0.02
✓	✓		✓	41.3 ± 1.9	59.9 ± 1.7	0.69 ± 0.01
✓	✓	✓		31.9 ± 2.0	47.2 ± 1.9	0.59 ± 0.01
			✓	2.6 ± 0.1	3.2 ± 0.1	0.80 ± 0.01

the LiDAR or RGB image modality significantly degrades *DS*, *RC*, and *IS* results. With only the language input, the model is nearly incapable of performing the driving task. This aligns with the fundamental role of human driving, where vision perception is essential. In addition, both the BEV tokens (planning) and the language modalities play an important role in ensuring strong driving performance.

C. Real-world Deployment

To validate the generalization capability of AppleVLM in the real world, we instantiate our model on an AGV platform without any fine-tuning by real-world driving data. Moreover, the sensor configurations are distinct from the ones used on the training data collected from the CARLA simulator. For safety concerns, we perform two handy closed-loop end-to-end driving tasks with dynamic obstacles such as random cyclists, pedestrians and vehicles around: 1) a 185 meters straight-line driving; 2) a 230-meter route includes both left and right turning. The end-to-end inference runs at 120 ms per frame (~ 8 FPS) on a single NVIDIA AGX Orin. The GPU utilization remains below 60% and the memory consumption is around 10 GB, which demonstrates the model’s efficiency on embedded hardware.

As demonstrated in Fig. 9, AppleVLM can complete two closed-loop end-to-end driving tasks without human takeover. Our model maintains driving without being disturbed by the surrounding obstacles. We provide a video in the supplementary materials to demonstrate the driving of AppleVLM in the real world. Note that there exists a significant domain gap between the CARLA simulation and the real-world environments, including object appearance, data distribution, sensor configuration, *etc.*, therefore, for learning-based models, sim-to-real has always been a critical yet unresolved challenge. Despite this, AppleVLM demonstrates promising generalization capability. Given that our method is simple and flexible, it would be interesting to explore it further in more complex

driving tasks and scenarios with advanced domain adaptation techniques.

VI. CONCLUSION

In this work, we propose a novel end-to-end model AppleVLM, that incorporates three modalities: vision, language, and planning for autonomous driving. We leverage the deformable transformer mechanism to enhance the vision encoder, enabling AppleVLM to be robust to variations in sensor configurations between training and real-world deployment. By fusing RGB images and point-cloud data in both spatial and temporal aspects, AppleVLM achieves higher driving and infraction scores on two CARLA driving benchmarks and shows a safer driving performance with fewer collisions. Compared to the traditional VLMs, we add the new planning modality to encode environmental spatial information provided by explicit BEVs that reduce language biases in navigation instruction. Furthermore, by fine-tuning the VLM backbone using corner cases through a CoT training mechanism, AppleVLM can effectively improve the generalization ability in out-of-distribution scenarios. Finally, real-world experiments validate the feasibility of directly deploying AppleVLM, trained in simulation, onto real vehicles without requiring domain adaptation.

REFERENCES

- [1] J. Zhao, W. Zhao, B. Deng, Z. Wang, F. Zhang, W. Zheng, W. Cao, J. Nan, Y. Lian, and A. F. Burke, “Autonomous driving system: A comprehensive survey,” *Expert Systems with Applications*, vol. 242, p. 122836, 2024.
- [2] S. Teng, X. Hu, P. Deng, B. Li, Y. Li, Y. Ai, D. Yang, L. Li, Z. Xuanyuan, F. Zhu *et al.*, “Motion planning for autonomous driving: The state of the art and future perspectives,” *IEEE Transactions on Intelligent Vehicles*, vol. 8, no. 6, pp. 3692–3711, 2023.
- [3] F. Codevilla, M. Müller, A. López, V. Koltun, and A. Dosovitskiy, “End-to-end driving via conditional imitation learning,” in *2018 IEEE international conference on robotics and automation (ICRA)*. IEEE, 2018, pp. 4693–4700.

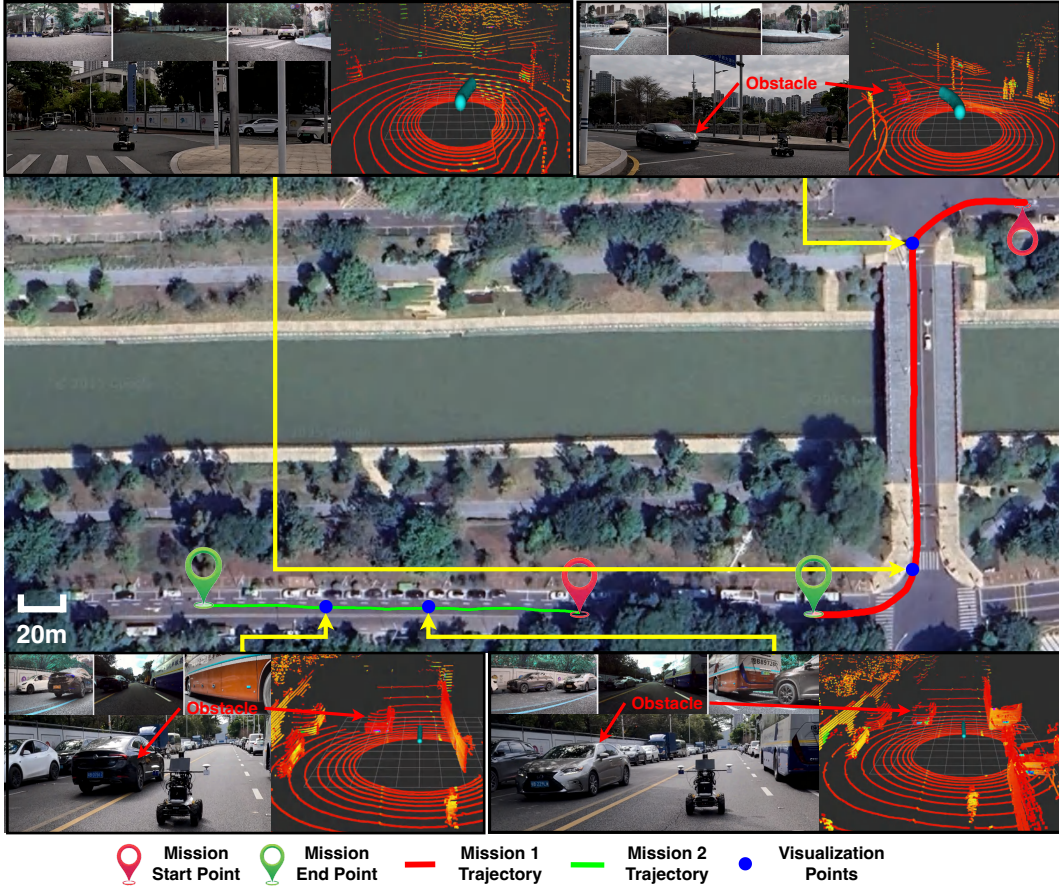


Fig. 9: The closed-loop driving in the real-world outdoor environment. The green line indicates the driving trajectory of *Going Straight* task, while the red one represents the driving trajectory of *Turning* task. Several waypoints (blue dots) are zoomed in to show the real driving environment (with dynamic pedestrians and vehicles around the ego vehicle).

- [4] Y. Hu, J. Yang, L. Chen, K. Li, C. Sima, X. Zhu, S. Chai, S. Du, T. Lin, W. Wang *et al.*, “Planning-oriented autonomous driving,” in *Proceedings of the IEEE/CVF Conference on Computer Vision and Pattern Recognition*, 2023, pp. 17 853–17 862.
- [5] P. S. Chib and P. Singh, “Recent advancements in end-to-end autonomous driving using deep learning: A survey,” *IEEE Transactions on Intelligent Vehicles*, vol. 9, no. 1, pp. 103–118, 2024.
- [6] Z. Zhang, A. Liniger, D. Dai, F. Yu, and L. Van Gool, “End-to-end urban driving by imitating a reinforcement learning coach,” in *Proceedings of the IEEE/CVF international conference on computer vision*, 2021, pp. 15 222–15 232.
- [7] Y. Lu, J. Fu, G. Tucker, X. Pan, E. Bronstein, R. Roelofs, B. Sapp, B. White, A. Faust, S. Whiteson *et al.*, “Imitation is not enough: Robustifying imitation with reinforcement learning for challenging driving scenarios,” in *2023 IEEE/RSJ International Conference on Intelligent Robots and Systems (IROS)*. IEEE, 2023, pp. 7553–7560.
- [8] L. Le Mero, D. Yi, M. Dianati, and A. Mouzakitis, “A survey on imitation learning techniques for end-to-end autonomous vehicles,” *IEEE Transactions on Intelligent Transportation Systems*, vol. 23, no. 9, pp. 14 128–14 147, 2022.
- [9] C. Pan, B. Yaman, T. Nesti, A. Mallik, A. G. Allievi, S. Velipasalar, and L. Ren, “Vlp: Vision language planning for autonomous driving,” in *Proceedings of the IEEE/CVF Conference on Computer Vision and Pattern Recognition*, 2024, pp. 14 760–14 769.
- [10] X. Zhou, M. Liu, E. Yurtsever, B. L. Zagar, W. Zimmer, H. Cao, and A. C. Knoll, “Vision language models in autonomous driving: A survey and outlook,” *IEEE Transactions on Intelligent Vehicles*, pp. 1–20, 2024.
- [11] A. Radford, J. W. Kim, C. Hallacy, A. Ramesh, G. Goh, S. Agarwal, G. Sastry, A. Askell, P. Mishkin, J. Clark *et al.*, “Learning transferable visual models from natural language supervision,” in *International conference on machine learning*. PMLR, 2021, pp. 8748–8763.
- [12] H. Touvron, L. Martin, K. Stone, P. Albert, A. Almahairi, Y. Babaei, N. Bashlykov, S. Batra, P. Bhargava, S. Bhosale *et al.*, “Llama 2: Open foundation and fine-tuned chat models,” *arXiv preprint arXiv:2307.09288*, 2023.
- [13] H. Liu, C. Li, Y. Li, and Y. J. Lee, “Improved baselines with visual instruction tuning,” *arXiv preprint arXiv:2310.03744*, 2024.
- [14] C. Cui, Y. Ma, X. Cao, W. Ye, Y. Zhou, K. Liang, J. Chen, J. Lu, Z. Yang, K.-D. Liao, T. Gao, E. Li, K. Tang, Z. Cao, T. Zhou, A. Liu, X. Yan, S. Mei, J. Cao, Z. Wang, and C. Zheng, “A Survey on Multimodal Large Language Models for Autonomous Driving,” in *2024 IEEE/CVF Winter Conference on Applications of Computer Vision Workshops (WACVW)*. Los Alamitos, CA, USA: IEEE Computer Society, Jan. 2024, pp. 958–979. [Online]. Available: <https://doi.ieeecomputersociety.org/10.1109/WACVW60836.2024.00106>
- [15] Z. Zhou, T. Cai, S. Z. Zhao, Y. Zhang, Z. Huang, B. Zhou, and J. Ma, “Autovla: A vision-language-action model for end-to-end autonomous driving with adaptive reasoning and reinforcement fine-tuning,” *arXiv preprint arXiv:2506.13757*, 2025.
- [16] X. Zhou, X. Han, F. Yang, Y. Ma, and A. C. Knoll, “Opendrivevla: Towards end-to-end autonomous driving with large vision language action model,” *arXiv preprint arXiv:2503.23463*, 2025.
- [17] S. Jiang, Z. Huang, K. Qian, Z. Luo, T. Zhu, Y. Zhong, Y. Tang, M. Kong, Y. Wang, S. Jiao *et al.*, “A survey on vision-language-action models for autonomous driving,” *arXiv preprint arXiv:2506.24044*, 2025.
- [18] H. Shao, Y. Hu, L. Wang, G. Song, S. L. Waslander, Y. Liu, and H. Li, “Lmdrive: Closed-loop end-to-end driving with large language models,” in *Proceedings of the IEEE/CVF Conference on Computer Vision and Pattern Recognition*, 2024, pp. 15 120–15 130.
- [19] L. Chen, O. Sinavski, J. Hünermann, A. Karnsund, A. J. Willmott, D. Birch, D. Maund, and J. Shotton, “Driving with llms: Fusing object-

level vector modality for explainable autonomous driving,” in *2024 IEEE International Conference on Robotics and Automation (ICRA)*. IEEE, 2024, pp. 14 093–14 100.

[20] X. Cao, T. Zhou, Y. Ma, W. Ye, C. Cui, K. Tang, Z. Cao, K. Liang, Z. Wang, J. M. Rehg *et al.*, “Maplm: A real-world large-scale vision-language benchmark for map and traffic scene understanding,” in *Proceedings of the IEEE/CVF conference on computer vision and pattern recognition*, 2024, pp. 21 819–21 830.

[21] B. Jaeger, K. Chitta, and A. Geiger, “Hidden biases of end-to-end driving models,” in *Proceedings of the IEEE/CVF International Conference on Computer Vision*, 2023, pp. 8240–8249.

[22] Y. A. Ozaiib, M. Dulva Hina, and A. Ramdane-Cherif, “End-to-end autonomous driving in carla: A survey,” *IEEE Access*, vol. 12, pp. 146 866–146 900, 2024.

[23] M. Zare, P. M. Kebria, A. Khosravi, and S. Nahavandi, “A survey of imitation learning: Algorithms, recent developments, and challenges,” *IEEE Transactions on Cybernetics*, vol. 54, no. 12, pp. 7173–7186, 2024.

[24] J. Chen, B. Yuan, and M. Tomizuka, “Deep imitation learning for autonomous driving in generic urban scenarios with enhanced safety,” in *2019 IEEE/RSJ international conference on intelligent robots and systems (IROS)*. IEEE, 2019, pp. 2884–2890.

[25] Y. Xiao, F. Codevilla, A. Gurrum, O. Urfalioglu, and A. M. López, “Multimodal end-to-end autonomous driving,” *IEEE Transactions on Intelligent Transportation Systems*, vol. 23, no. 1, pp. 537–547, 2022.

[26] Y. Xiao, F. Codevilla, D. Porres, and A. M. López, “Scaling vision-based end-to-end autonomous driving with multi-view attention learning,” in *2023 IEEE/RSJ International Conference on Intelligent Robots and Systems (IROS)*, 2023, pp. 1586–1593.

[27] K. Chitta, A. Prakash, B. Jaeger, Z. Yu, K. Renz, and A. Geiger, “Transfuser: Imitation with transformer-based sensor fusion for autonomous driving,” *IEEE Transactions on Pattern Analysis and Machine Intelligence*, vol. 45, no. 11, pp. 12 878–12 895, 2023.

[28] H. Shao, L. Wang, R. Chen, H. Li, and Y. Liu, “Safety-enhanced autonomous driving using interpretable sensor fusion transformer,” in *Conference on Robot Learning*. PMLR, 2023, pp. 726–737.

[29] P. Wu, X. Jia, L. Chen, J. Yan, H. Li, and Y. Qiao, “Trajectory-guided control prediction for end-to-end autonomous driving: A simple yet strong baseline,” *Advances in Neural Information Processing Systems*, vol. 35, pp. 6119–6132, 2022.

[30] X. Jia, Z. Yang, Q. Li, Z. Zhang, and J. Yan, “Bench2drive: Towards multi-ability benchmarking of closed-loop end-to-end autonomous driving,” in *NeurIPS 2024 Datasets and Benchmarks Track*, 2024.

[31] Y. Ma, W. Ye, C. Cui, H. Zhang, S. Xing, F. Ke, J. Wang, C. Miao, J. Chen, H. Rezatofighi *et al.*, “Position: Prospective of autonomous driving-multimodal llms world models embodied intelligence ai alignment and mamba,” in *Proceedings of the Winter Conference on Applications of Computer Vision*, 2025, pp. 1010–1026.

[32] C. Cui, Y. Ma, X. Cao, W. Ye, and Z. Wang, “Receive, reason, and react: Drive as you say, with large language models in autonomous vehicles,” *IEEE Intelligent Transportation Systems Magazine*, vol. 16, no. 4, pp. 81–94, 2024.

[33] C. Cui, Z. Yang, Y. Zhou, J. Peng, S.-Y. Park, C. Zhang, Y. Ma, X. Cao, W. Ye, Y. Feng *et al.*, “On-board vision-language models for personalized autonomous vehicle motion control: System design and real-world validation,” *arXiv preprint arXiv:2411.11913*, 2024.

[34] Z. Xu, Y. Zhang, E. Xie, Z. Zhao, Y. Guo, K.-Y. K. Wong, Z. Li, and H. Zhao, “Drivegpt4: Interpretable end-to-end autonomous driving via large language model,” *IEEE Robotics and Automation Letters*, vol. 9, no. 10, pp. 8186–8193, 2024.

[35] C. Sima, K. Renz, K. Chitta, L. Chen, H. Zhang, C. Xie, J. Beißwenger, P. Luo, A. Geiger, and H. Li, “Drivelm: Driving with graph visual question answering,” in *European Conference on Computer Vision*. Springer, 2025, pp. 256–274.

[36] X. Tian, J. Gu, B. Li, Y. Liu, Y. Wang, Z. Zhao, K. Zhan, P. Jia, X. Lang, and H. Zhao, “Drivevlm: The convergence of autonomous driving and large vision-language models,” *arXiv preprint arXiv:2402.12289 (Computer Science, Vision)*, 2024.

[37] X. Zhu, W. Su, L. Lu, B. Li, X. Wang, and J. Dai, “Deformable detr: Deformable transformers for end-to-end object detection,” *arXiv preprint arXiv:2010.04159*, 2020.

[38] T. Mikolov, “Efficient estimation of word representations in vector space,” *arXiv preprint arXiv:1301.3781*, vol. 3781, 2013.

[39] W. Ding, L. Zhang, J. Chen, and S. Shen, “Epsilon: An efficient planning system for automated vehicles in highly interactive environments,” *IEEE Transactions on Robotics*, vol. 38, no. 2, pp. 1118–1138, 2022.

[40] T.-B. Li, A.-A. Liu, D. Song, W.-H. Li, J. Zhang, Z.-Q. Wei, and Y.-T. Su, “Multi-task spatial-temporal transformer for multi-variable meteorological forecasting,” *IEEE Transactions on Knowledge and Data Engineering*, vol. 36, no. 12, pp. 8876–8888, 2024.

[41] J. Li, D. Li, S. Savarese, and S. Hoi, “Blip-2: Bootstrapping language-image pre-training with frozen image encoders and large language models,” in *International conference on machine learning*. PMLR, 2023, pp. 19 730–19 742.

[42] X. Chen, Z. Wu, X. Liu, Z. Pan, W. Liu, Z. Xie, X. Yu, and C. Ruan, “Janus-pro: Unified multimodal understanding and generation with data and model scaling,” *arXiv preprint arXiv:2501.17811*, 2025.

[43] Y. Li, W. Zhang, K. Chen, Y. Liu, P. Li, R. Gao, L. Hong, M. Tian, X. Zhao, Z. Li *et al.*, “Automated evaluation of large vision-language models on self-driving corner cases,” *arXiv preprint arXiv:2404.10595*, 2024.

[44] B. Bamieh, F. Paganini, and M. Dahleh, “Distributed control of spatially invariant systems,” *IEEE Transactions on Automatic Control*, vol. 47, no. 7, pp. 1091–1107, 2002.

[45] A. Dosovitskiy, G. Ros, F. Codevilla, A. Lopez, and V. Koltun, “CARLA: An open urban driving simulator,” in *Proceedings of the 1st Annual Conference on Robot Learning*, 2017, pp. 1–16.

[46] J. Xu, Y. Pan, X. Pan, S. Hoi, Z. Yi, and Z. Xu, “Regnet: Self-regulated network for image classification,” *IEEE Transactions on Neural Networks and Learning Systems*, vol. 34, no. 11, pp. 9562–9567, 2023.

[47] I. Loshchilov and F. Hutter, “Decoupled weight decay regularization,” *arXiv preprint arXiv:1711.05101 (Computer Science, Learning)*, 2019.

[48] I. Loshchilov, “Sgdr: Stochastic gradient descent with warm restarts,” *arXiv preprint arXiv:1608.03983 (Computer Science, Learning)*, 2017.

[49] H. Liu, C. Li, Y. Li, B. Li, Y. Zhang, S. Shen, and Y. J. Lee, “Llava-next: Improved reasoning, ocr, and world knowledge,” January 2024. [Online]. Available: <https://llava-vl.github.io/blog/2024-01-30-llava-next/>

[50] Z. Li, W. Wang, H. Li, E. Xie, C. Sima, T. Lu, Y. Qiao, and J. Dai, “Bevformer: Learning bird’s-eye-view representation from multi-camera images via spatiotemporal transformers,” in *European conference on computer vision*. Springer, 2022, pp. 1–18.

[51] M. Mo, J. Wang, L. Wang, H. Chen, C. Gu, J. Leng, and X. Gao, “NexusAD: Exploring the nexus for multimodal perception and comprehension of corner cases in autonomous driving,” in *ECCV 2024 Workshop on Multimodal Perception and Comprehension of Corner Cases in Autonomous Driving*, 2024. [Online]. Available: <https://openreview.net/forum?id=LXZO1nGI0d>

[52] Y. Xue, H. Zhang, Y. Zhu, W. Zhou, S. Cui, and Z. Li, “Two-stage LVL system: 1st place solution for ECCV 2024 corner case scene understanding challenge,” in *ECCV 2024 Workshop on Multimodal Perception and Comprehension of Corner Cases in Autonomous Driving*, 2024. [Online]. Available: <https://openreview.net/forum?id=Or6HZXwvra>